

Analytical Methods

Accepted Manuscript



This is an *Accepted Manuscript*, which has been through the Royal Society of Chemistry peer review process and has been accepted for publication.

Accepted Manuscripts are published online shortly after acceptance, before technical editing, formatting and proof reading. Using this free service, authors can make their results available to the community, in citable form, before we publish the edited article. We will replace this *Accepted Manuscript* with the edited and formatted *Advance Article* as soon as it is available.

You can find more information about *Accepted Manuscripts* in the [Information for Authors](#).

Please note that technical editing may introduce minor changes to the text and/or graphics, which may alter content. The journal's standard [Terms & Conditions](#) and the [Ethical guidelines](#) still apply. In no event shall the Royal Society of Chemistry be held responsible for any errors or omissions in this *Accepted Manuscript* or any consequences arising from the use of any information it contains.

1
2
3
4 **Highly-sensitive electrochemical detection of bisphenol A based on**
5
6 **the cooperative enhancement effect of graphene-Ni(OH)₂ hybrid and**
7
8 **hexadecyltrimethylammonium bromide**
9

10
11
12
13
14 ¹Rui Wang ^a, Kangbing Wu ^b, Can Wu ^{b*}
15
16
17

18
19 ^a Wuhan Second Ship Design and Research Institute, Wuhan 430205, China
20

21 ^b School of Chemistry and Chemical Engineering, Huazhong University of Science
22
23 and Technology, Wuhan 430074, China
24
25
26
27

28
29 Graphene sheets (GS) are first easily prepared *via* one-step solvent exfoliation of
30 graphite powder in N-methyl-2-pyrrolidone (NMP) and then hybridizes with Ni(OH)₂
31 microparticles. The resulting insoluble GS-Ni(OH)₂ hybrid is readily dispersed in
32 water in the presence of surfactant hexadecyltrimethylammonium bromide (CTAB).
33
34 Compared with the bare glassy carbon electrode (GCE), CTAB, pristine GS, Ni(OH)₂,
35 and GS-Ni(OH)₂ composite modified GCEs shows enhanced oxidation signal for
36 bisphenol A (BPA). Based on the cooperative enhancement effect of
37 solvent-exfoliated graphene-Ni(OH)₂ hybrid and CTAB, a novel electrochemical
38 sensor with high sensitivity is developed for the detection of BPA. Under the optimal
39 conditions, the detection limit (S/N =3) is estimated to be as low as 5.0 nM. In the end,
40
41
42
43
44
45
46
47
48
49
50
51
52
53
54
55
56
57

58
59
60

* Corresponding author. *E-mail address:* cwu@hust.edu.cn

1
2
3
4 the fabricated electrochemical sensor is successfully used to determine the content of
5
6 BPA in real water samples.
7
8
9

10
11 **Keywords:** Graphene; Ni(OH)₂; Bisphenol A; Electrochemical sensor
12
13

14 15 **Introduction**

16
17 Bisphenol A (BPA, 2,2-bis (4-hydroxyphenyl) propane) is a common industrial
18
19 monomer compound for the synthesis of polycarbonate, polystyrene resins, and epoxy
20
21 resin, which are widely applied to produce daily plastic products. More and more
22
23 studies show that BPA is a kind of endocrine disruptor chemical that may potentially
24
25 interfere the endocrine system of both the wildlife and human. Intake of low dose of
26
27 BPA may induce cancer,¹ decrease semen quality,² reduce immune function,³ lead to
28
29 learning deficits,⁴ and impair reproduction.⁵ Due to the daily use of plastic products
30
31 such as plastic bag, plastic bottle, plastic toy and so on, humans may indirectly ingest
32
33 trace amount of BPA. So it is of great importance to develop a fast and sensitive
34
35 detection platform for monitoring the content of BPA.
36
37
38
39
40
41
42

43
44 Graphene, a two-dimensional and one-atom thick carbon sheet, has received
45
46 considerable attention due to its unique physical properties.⁶⁻⁸ Especially in these
47
48 years, multifarious graphene-based electrochemical sensors with low detection limit,
49
50 high sensitivity and reduced resistance have emerged.⁹⁻¹³ However, among these
51
52 studies, graphene was predominantly obtained *via* chemical oxidation exfoliation of
53
54 graphite according to modified Hummer's methods, which involve the consumption of
55
56
57
58
59
60

1
2
3
4 a large amount of strong oxidizing reagents, complicated and rigorous treatments, and
5
6 irreversible structure defects. Therefore, it is necessary to prepare graphene through a
7
8 simple, eco-friendly, and mild method with high quality. Recently, one-step solvent
9
10 sonication exfoliation method has been proved to be feasible for preparation of
11
12 pristine graphene.^{14,15} However, the solvent exfoliated graphene-based
13
14 electrochemical is still very limited.
15
16
17

18
19 On the other hand, nano metal and metal oxide, such as Au,¹⁶ Ag,¹⁷ CuO,¹⁸
20
21 Fe₂O₃,¹⁹ Ni(OH)₂,²⁰ TiO₂²¹ and so on, are frequently used to enhance the
22
23 electrochemical performance of graphene. In these graphene-based hybrid materials,
24
25 Ni(OH)₂ has gained considerable attention due to its high stability, large proton
26
27 diffusion coefficient²² and strong catalytic reaction activity²³.
28
29
30

31
32 In this work, graphene sheets (GS) are easily prepared *via* one-step solvent
33
34 exfoliation of graphite powder in N-methyl-2-pyrrolidone (NMP). The Ni(OH)₂
35
36 microparticles are synthesized by simple homogeneous precipitation method.
37
38 Considering the insolubility of GS and Ni(OH)₂, CTAB, a common cationic surfactant,
39
40 is selected as the dispersing agent. After then, GS-Ni(OH)₂ hybrid is used to modify
41
42 the surface of glassy carbon electrode (GCE). The electrochemical behaviors of BPA
43
44 on the surface of bare GCE, CTAB-modified GCE (CTAB/GCE), Ni(OH)₂-modified
45
46 GCE (Ni(OH)₂/GCE), GS-modified GCE (GS/GCE), and GS-Ni(OH)₂
47
48 composite-modified GCE (GS-Ni(OH)₂/GCE) are systematically studied. CTAB/GCE,
49
50 Ni(OH)₂/GCE and GS/GCE shows an obvious signal enhancement responding to BPA
51
52 oxidation compared with bare GCE, and the oxidation peak current is further
53
54
55
56
57
58
59
60

1
2
3 increased on GS-Ni(OH)₂/GCE. Such remarkable enhancement effect for BPA
4
5 oxidation may be attributed to the cooperative enhancement effect of GS-Ni(OH)₂
6
7 hybrid and CTAB, which leads to the notably improved accumulation efficiency of
8
9 BPA. Therefore, a novel and simple electrochemical sensing platform is successfully
10
11 fabricated for BPA detection. Compared with the reported electrochemical methods
12
13 for BPA detection, this newly fabricated sensing platform for BPA exhibits higher
14
15 sensitivity, as confirmed from Table 1.
16
17
18
19
20
21

22 **Experimental Section**

23 **Reagents**

24
25 All chemicals are of analytical grade and used as received. BPA (Sigma) is dissolved
26
27 into ethanol to prepare 0.01 M standard solution. Graphite powder (spectral pure),
28
29 NMP, Ni(NO₃)₂, NH₃·H₂O (28 wt%), CTAB are purchased from Sinopharm Chemical
30
31 Reagent Company (Shanghai, China). Ultrapure water (18.2 MΩ) is obtained from a
32
33 Milli-Q water purification system and used throughout.
34
35
36
37
38
39
40
41

42 **Instruments**

43
44 Electrochemical measurements are performed on a CHI 660D electrochemical
45
46 workstation (Chenhua Instrument, Shanghai, China). The working electrode is a
47
48 glassy carbon electrode (GCE), the reference electrode is a calomel electrode with
49
50 saturated KCl, and the counter electrode is a Pt wire. Scanning electron microscopy
51
52 (SEM) is performed with a Nova NanoSEM450 microscope (FEI Company,
53
54 Netherlands). Transmission electron microscopy (TEM) image is taken using a Tecnai
55
56
57
58
59
60

1
2
3
4 G220 microscope (FEI Company, Netherlands). X-ray diffraction (XRD) pattern is
5
6 conducted using a X'Pert PRO diffractometer (Panalytical Company, Netherlands).
7
8
9

10 11 **Preparation of GS and GS-Ni(OH)₂ hybrid**

12
13 GS are easily prepared *via* one-step ultrasonic exfoliation of graphite powder in NMP
14
15 solvent. In a typical preparation, 5.0 g graphite powder is added into 500.0 mL NMP,
16
17 and then sonicates in a KQ-100B ultrasonicator (frequency: 40 kHz, power: 100 W;
18
19 Kunshan Ultrasonic Instrument Co., Ltd, China) for 48 h. The resulting suspension is
20
21 denoted as graphite@48 h. After that, the suspension is centrifugated, washed with
22
23 ultrapure water and ethanol several times, and finally dried in vacuum at 60 °C for 5
24
25
26
27
28
29 h.

30
31 Ni(OH)₂ microparticles are prepared by simple homogeneous precipitation
32
33 method. Firstly, 23.2 g Ni(NO₃)₂ is dissolved in 20 mL distilled water, then the
34
35 Ni(NO₃)₂ solution is added into a beaker containing 40 mL ammonia solution (28
36
37 wt%) under magnetic stirring drop by drop at room temperature. After that, the mixed
38
39 solution is transferred to a water bath with continuous magnetic stirring at 70 °C for
40
41 18 h. Finally, after aging the product in mother liquor for 6 h, the light green
42
43 precipitate is collected by centrifugation, washed with ultrapure water several times,
44
45 and dried at 100 °C in vacuum for 8 h.
46
47
48
49
50

51
52 For the preparation of GS-Ni(OH)₂ hybrid, 10.0 mg GS and 10.0 mg Ni(OH)₂
53
54 are first exactly weighed, and then together added in 5 mL, 1 mg/mL CTAB solution.
55
56
57
58
59
60

1
2
3
4 After 30-min ultrasonic treatment, a stable black suspension with concentration of 2
5
6 mg/mL GS-Ni(OH)₂ composite is obtained.
7
8
9

10 11 **Fabrication of modified GCEs**

12
13 GCE with diameter of 3 mm is polished with 0.05 μm alumina slurry, and then
14
15 sonicated in ultrapure water to give a clean surface. After being dried, a certain
16
17 amount of GS-Ni(OH)₂ suspension is coated on GCE surface, and then dried under an
18
19 infrared lamp in air. For the comparison, GS and Ni(OH)₂ are also dispersed in CTAB
20
21 solution and used to modify the GCE according to the above procedure. The
22
23 CTAB-modified GCE is similarly prepared using 1 mg/mL CTAB solution.
24
25
26
27
28
29
30

31 **Analytical procedure**

32
33 0.1 M phosphate buffer solution (pH 7.5) is used as the supporting electrolyte. After
34
35 accumulation at 0.2 V under stirring for 180 s, differential pulse voltammetry (DPV)
36
37 curves are recorded by applying a positive-going scan from 0.2 to 0.8 V, and the
38
39 oxidation peak current at 0.49 V is measured. The pulse amplitude was 50 mV, the
40
41 step increment was 4 mV, the pulse width was 40 ms, the sampling width is 16.7 ms
42
43 and the scan rate is 40 mV/s.
44
45
46
47
48
49
50

51 **Results and discussion**

52 53 54 55 56 **Morphology and structure characterization** 57 58 59 60

1
2
3
4 In order to verify the bulk graphite is effectively exfoliated into graphene nanoflakes,
5
6 SEM and TEM characterization of bulk graphite and graphite@48 h are conducted.
7
8 As shown in Fig. 1A, the pristine graphite is consisted of large number of bulk
9
10 particles on a micron meter scale. After applying graphene suspension that
11
12 ultrasonically exfoliated for 48 h in NMP, plenty of graphene nanoflakes are observed,
13
14 indicating graphite is effectively exfoliated (Fig. 1B). In addition, many transparent
15
16 nanosheets can be seen from the TEM image of graphite@48 h (Fig. 1C). Apparently,
17
18 graphene has been successfully obtained through the ultrasonic exfoliation of graphite
19
20 powder in NMP.
21
22
23
24
25

26 Raman spectra measurements and XRD tests are also conducted to provide
27
28 further insights into the structural differences of graphite and graphite@48 h. As
29
30 displayed in Fig. 2A, three peaks at 1350 cm^{-1} , 1580 cm^{-1} and 2700 cm^{-1} are easily
31
32 observed with the graphite powder and graphite@48 h, which can be attributed to the
33
34 natural D-band, G-band and 2D-band of carbon material, respectively. D-band is
35
36 assigned to the disorder-related peak, which is due to the existence of defects in basal
37
38 plane and edge of carbon material.^{34,35} The peak intensity ratio of I_D/I_G is often used
39
40 to evaluate the surface defect level of carbon material. Obviously, the D-band
41
42 intensities of graphite@48 h is significantly enhanced relative to pristine graphite,
43
44 demonstrating a highly-effective exfoliation of bulk graphite and the generation of
45
46 graphene. Moreover, for graphite@48 h, the intensity of the characteristic diffraction
47
48 peak (002) of carbon material decreases greatly compared with pristine graphite,
49
50 which suggests the wide-range periodicity associated with the stacking of graphene in
51
52
53
54
55
56
57
58
59
60

1
2
3
4
5
6
7
8
9
10
11
12
13
14
15
16
17
18
19
20
21
22
23
24
25
26
27
28
29
30
31
32
33
34
35
36
37
38
39
40
41
42
43
44
45
46
47
48
49
50
51
52
53
54
55
56
57
58
59
60

graphite has been destroyed by ultrasound exfoliation. So it can be concluded that graphene is obtained *via* one-step solvent exfoliation of graphite powder in NMP and this result has also been confirmed in our previous work.^{36,37}

The surface morphology of different electrodes are characterized using SEM, and the results are shown in Fig. 3. As seen in Fig. 3A, a thin film is formed on the surface of CTAB-modified GCE. After modification with GS (B), the GCE surface is covered by a large number of nanosheets. The nanosheets indicates the bulk graphite powder is effectively exfoliated to graphene. On the surface of Ni(OH)₂/GCE (C), corrugated appearance is observed, indicating high roughness of Ni(OH)₂. Inset in Fig. C is the low magnification of SEM image of Ni(OH)₂, it is clear that the obtained Ni(OH)₂ samples are composed of numerous of corrugated structure with micron-scale. In addition, the wrinkled structure is clearly found on the surface of graphene-Ni(OH)₂ composite (D), suggesting the graphene nanosheets are successfully hybridized with Ni(OH)₂. From the comparison, it is apparent that the GS-Ni(OH)₂ hybrid owns larger surface roughness and three-dimensional structure.

Furthermore, the crystal structure and the phase purity of the as-synthesized Ni(OH)₂ is examined using XRD. As shown in Fig. 4, characteristic diffraction peaks of (003), (006), (101), (015), (018), (110) and (113) can be readily indexed as the α -Ni(OH)₂ structure (JCPDS No. 38-0715).³⁸ In addition, no diffraction peaks from impurities could be founded from the XRD image of Ni(OH)₂, indicating the high purity of the resulting sample.

Cooperative enhancement effect of GS-Ni(OH)₂ and CTAB for BPA response

Fig. 5A shows the DPV curves of 0.5 μM BPA at different electrodes and Fig. 5B illustrates the corresponding variation of oxidation peak current. A negligible oxidation peak is observed at bare GCE (a), indicating poor accumulation ability of bare GCE. When using CTAB/GCE (b), the oxidation signal of BPA at 0.49 V can be seen, suggesting CTAB is conducive to the detection of BPA. This declares that surfactant can also be electrocatalytic active.³⁹ The oxidation signal further increases at Ni(OH)₂/GCE (curve c), suggesting its high electrochemical activity toward the oxidation of BPA. This enhanced oxidation signal may be attributed to the rough surface of Ni(OH)₂. It is noticed that the oxidation peak current of BPA increases greatly on GS/GCE (curve d), indicating the prepared GS displays strong catalytic activity on BPA oxidation. Interestingly, GS-Ni(OH)₂ hybrid film shows the highest oxidation current (curve e). In conclusion, the arresting signal amplification may be due to the cooperative enhancement effect of GS-Ni(OH)₂ hybrid and CTAB, which leads to the remarkably increased accumulation efficiency for BPA.

Detection of BPA

Fig. 6A shows the effect of electrolyte pH on the current of 100 μM BPA on GS-Ni(OH)₂/GCE. Different pH values containing 0.1 M phosphate buffer solution with pH of 6, 6.5, 7, 7.5, 8 and 9.15 are tested using cyclic voltammetry (CV) with scan rate of 100 mV/s. As seen in Fig. 6A, only an oxidation peak is observed during the cyclic sweep from 0.2 to 0.8 V, revealing the oxidation of BPA on GS-Ni(OH)₂

1
2
3
4 hybrid film is totally irreversible. In addition, the oxidation peak current of BPA
5
6 increases gradually with the increase of the pH from 6 to 7.5. When further improving
7
8 pH value to 9.15, the oxidation signal decreases gradually. Thus, 0.1 M phosphate
9
10 buffer solution solution with pH of 7.5 is selected for BPA detection in the following
11
12 study.
13
14

15
16 The effect of the accumulation potential on the oxidation signal of 0.5 μM BPA
17
18 is studied in the range from -0.2 V to 0.4 V using DPV, and the results are shown in
19
20 Fig. 6B. When the accumulation potential shifts toward positive from -0.2 V to 0.2 V,
21
22 the oxidation peak current of BPA increases greatly. When further moving the
23
24 potential to 0.4 V, the peak current of BPA starts to decrease gradually. So 0.2 V is
25
26 selected as the optimum accumulation potential for further measurements.
27
28
29

30
31 Fig. 6C shows the dependence of the oxidation signal of 0.5 μM BPA on the
32
33 amount of graphene suspension. As illustrated in Fig. 6C, the oxidation peak current
34
35 increases remarkably with the volume of graphene suspension over the range from 0
36
37 to 2 μL , indicating an improved enhancement effect. When further extending the
38
39 volume to 5 μL , the oxidation signal decreases remarkably, this may be attributed to
40
41 the increase of nonconducting surfactant and $\text{Ni}(\text{OH})_2$ hinders the electron transfer.
42
43 For the highest sensitivity, 2 μL graphene suspension is used.
44
45
46
47

48
49 The effect of the accumulation time on the oxidation peak current of 0.5 μM BPA
50
51 is studied under the optimized conditions described above. As can be seen from Fig.
52
53 6D, the oxidation peak current of BPA increases linearly with extending the
54
55 accumulation time in the range of 0 to 180 s, this phenomenon suggests that
56
57
58
59
60

1
2
3
4 accumulation is rather efficient to improve the detection sensitivity. However, when
5
6 further prolonging the accumulation time to 300 s, the increasing tendency of the
7
8 oxidation current is not so obvious, suggesting the adsorption of BPA on the electrode
9
10 surface tends to a limit value. In order to guarantee the detection sensitivity while
11
12 keeping high detection efficiency of the sensor, an accumulation time of 180 s is
13
14
15 chosen.

16
17
18 In this work, we find that the GS-Ni(OH)₂-modified GCE is unqualified for the
19
20 successive measurements because the oxidation peak currents of BPA increases
21
22 continuously. Thus, it is just employed for the single measurement. The
23
24 reproducibility between eleven GS-Ni(OH)₂ modified GCEs is investigated based on
25
26 the oxidation signal of 0.5 μM BPA. Each electrode undergoes one measurement and
27
28 the resulting value of relative standard deviation (RSD) is 4.5%, suggesting excellent
29
30 fabrication reproducibility and good detection precision.

31
32
33 The potential interferents are also studied for the detection of BPA. Under the
34
35 optimized conditions, the oxidation peak current of 0.5 μM BPA is measured after
36
37 adding different concentrations of interferents, the interferents are added individually
38
39 and the peak current change is then checked. It is found that 1000-fold amounts of
40
41 Ca²⁺, Mg²⁺, K⁺, Cl⁻, SO₄²⁻, NO₃⁻, CO₃²⁻, 80-fold amounts of o-nitrophenol,
42
43 m-nitrophenol, p-nitrophenol, phenol, catechol, hydroquinone and 30 -fold amounts
44
45 of o-aminophenol, m-aminophenol and p-aminophenol have no influence on the
46
47 detection of BPA when the signals change are below 10%.

48
49
50 The linear range and detection limit for BPA are also examined using DPV under
51
52
53
54
55
56
57
58
59
60

1
2
3
4 the optimized conditions. As shown in Fig. 7, the oxidation peak current of BPA (I_p ,
5 μA) is proportional to its concentration (C , nM) over the range from 10 nM to 2000
6 nM. The calibration curve and correlation coefficients are $I_p(\mu\text{A}) = 0.0046 C(\text{nM})$, $R =$
7
8 0.998. In addition, the oxidation signals of 10 nM BPA at GS-Ni(OH)₂ are recorded to
9 estimate its detection limit. The standard deviation of eleven detection is calculated,
10 and the limit of detection (LOD) for BPA is evaluated to be as low as 5 nM based on a
11 signal to noise ratio of 3 with an accumulation time of 180 s.
12
13
14
15
16
17
18
19
20
21
22
23

24 Analytical application

25
26 In order to evaluate the sensing performance of this method, the fabricated
27 GS-Ni(OH)₂/GCE is used to determine BPA content in the real water samples. In brief,
28 water samples collected from different place in Wuhan city are first filtered through a
29 0.45 μm filter membrane. Then, 5.0 mL of water sample is added into 5.0 mL pH 7.5
30 phosphate buffer solution. Afterward, the DPV curves are recorded from 0.2 to 0.8 V
31 after accumulation for 180 s. The results illustrated in Table 2. show that no BPA is
32 detected in these water samples. So the BPA standards with different concentrations
33 are spiked into the water samples. Each water sample undergoes three parallel
34 detections, and the RSD value is below 5%, suggesting high detection precision. The
35 content of BPA in water samples are calculated by standard addition method, and the
36 results are listed in Table 1. The value of recovery is in the range from 97.0% to
37 105.0%, revealing the newly-developed method is accurate and has promising
38 application.
39
40
41
42
43
44
45
46
47
48
49
50
51
52
53
54
55
56
57
58
59
60

Conclusions

Graphene nanosheets are easily prepared *via* one-step solvent exfoliation of graphite powder and high surface roughness of wrinkled Ni(OH)₂ are synthesized by simple homogeneous precipitation method. The fabricated graphene-Ni(OH)₂ hybrid sensing film exhibits stronger signal enhancement on BPA oxidation, relative to pristine graphene and pure Ni(OH)₂. The remarkably enhanced BPA oxidation signal may be attributed to the cooperative enhancement effect of GS-Ni(OH)₂ hybrid and CTAB, which leads to the notably increased accumulation efficiency for BPA. Compared with the reported electrochemical methods for BPA detection, this newly fabricated sensing platform for BPA exhibits higher sensitivity. Furthermore, this analytic method is successfully applied to detect the trace level of BPA in the real samples.

Acknowledgements

This work was supported by the National Natural Science Foundation of China (Grant No. 21375041) and the Program for New Century Excellent Talents in University (Grant NCET-11-0187). The Center of Analysis and Testing of Huazhong University of Science and Technology was also acknowledged for its help in the SEM, TEM observation and XRD test.

References

- 1 S. Jenkins, N. Raghuraman, I. Eltoum, M. Carpenter, J. Russo, C.A. Lamartiniere, *Environ. Health Perspect.*, 2009, **117**, 910-915.
- 2 M.V. Maffini, B.S. Rubin, C. Sonnenschein, A.M. Soto, *Mol. Cell. Endocrinol.*, 2006, **254**, 179-186.
- 3 J.A. Rogers, L. Metz, V.W. Yong, *Mol. Immunol.*, 2013, **53**, 421-430.
- 4 K.S. Saili, M.M. Corvi, D.N. Weber, A.U. Patel, S.R. Das, J. Przybyla, K.A. Anderson, R.L. Tanguay, *Toxicology*, 2012, **291**, 83-92.
- 5 P.A. Hunt, M. Susiarjo, C. Rubio, T.J. Hassold, *Biol. Reprod.*, 2009, **81**, 807-813.
- 6 A.A. Balandin, *Nat. Mater.*, 2011, **10**, 569-581.
- 7 A.H. Castro Neto, F. Guinea, N.M.R. Peres, K.S. Novoselov, A.K. Geim, *Rev. Mod. Phys.*, 2009, **81**, 109-162.
- 8 A.K. Geim, K.S. Novoselov, *Nat. Mater.*, 2007, **6**, 183-191.
- 9 L. Wang, M. Xu, L. Han, M. Zhou, C.Z. Zhu, S.J. Dong, *Anal. Chem.*, 2012, **84**, 7301-7307.
- 10 J.F. Wu, M.Q. Xu, G.C. Zhao, *Electrochem. Commun.*, 2010, **12**, 175-177.
- 11 Q.J. Wan, Y. Liu, Z.H. Wang, W. Wei, B.B. Li, J. Zou, N.J. Yang, *Electrochem. Commun.*, 2013, **29**, 29-32.
- 12 Q.J. Wan, H. Cai, Y. Liu, H.T. Song, H.L. Liao, S.T. Liu, N.J. Yang, *Chem. Eur. J.*, 2013, **19**, 3483-3489.
- 13 X. Luo, Z.P. Qiu, Q.J. Wan, H. Shu, N.J. Yang, *Phys. Status Solidi A-Appl. Mat.*, 2014, **12**, 2795-2800.

- 1
2
3
4 14 Y. Hernandez, V. Nicolosi, M. Lotya, F.M. Blighe, Z.Y. Sun, S. De, I.T. Mcgovern,
5
6 B. Holland, M. Byrne, Y.K. Gun'ko, J.J. Boland, P. Niraj, G. Duesberg, S.
7
8 Krishnamurthy, R. Goodhue, J. Hutchison, V. Scardaci, A.C. Ferrari, J.N.
9
10 Coleman, *Nat. Nanotechnol.*, 2008, **3**, 563-568.
11
12
13
14 15 J.N. Coleman, *Adv. Funct. Mater.*, 2009, **19**, 3680-3695.
15
16
17 16 K.F. Zhou, Y.H. Zhu, X.L. Yang, J. Luo, C.Z. Li, S.R. Luan, *Electrochim. Acta*,
18
19 2010, **55**, 3055-3060.
20
21
22 21 Y.W. Zhang, S. Liu, L. Wang, X.Y. Qin, J.Q. Tian, W.B. Lu, G.H. Chang, X.P. Sun,
23
24 *RSC Adv.*, 2012, **2**, 538-545.
25
26
27 18 Y.W. Hsu, T.K. Hsu, C.L. Sun, Y.T. Nien, N.W. Pu, M.D. Ger, *Electrochim. Acta*,
28
29 2012, **82**, 152-157.
30
31
32 19 C. Wu, Q. Cheng, L.Q. Li, J.P. Chen, K.B. Wu, *Electrochim. Acta*, 2014, **115**,
33
34 434-439.
35
36
37 20 Y. Zhang, F.G. Xu, Y.J. Sun, Y. Shi, Z.W. Wen, Z. Li, *J. Mater. Chem.*, 2011, **21**,
38
39 16949-16954.
40
41
42 21 Y. Fan, H.T. Lu, J.H. Liu, C.P. Yang, Q.S. Jing, Y.X. Zhang, X.K. Yang, K.J. Huang,
43
44 *Colloid Surf. B-Biointerfaces*, 2011, **83**, 78-82.
45
46
47 22 X.J. Han, P. Xu, C.Q. Xu, L. Zhao, Z.B. Mo, T. Liu, *Electrochim. Acta*, 2005, **50**,
48
49 2763-2769.
50
51
52 23 G.M. Wang, Y.C. Ling, X.H. Lu, T. Zhai, F. Qian, Y.X. Tong, Y. Li, *Nanoscale*,
53
54 2013, **5**, 4129-4133.
55
56
57
58
59
60

- 1
2
3
4 24 B. Ntsendwana, B.B. Mamba, S. Sampath, O.A. Arotiba, *Int. J. Electrochem. Sci.*,
5
6 2012, **7**, 3501-3512.
7
8
9 25 L. Peng, S.Y. Dong, H.D. Xie, G.Z. Gu, Z.X. He, J.S. Lu, T.L. Huang, *J.*
10
11 *Electroanal. Chem.*, 2014, **726**, 15-20.
12
13
14 26 F.R. Wang, J.Q. Yang, K.B. Wu, *Anal. Chim. Acta*, 2009, **638**, 23-28.
15
16
17 27 Y.Q. Lin, K.Y. Liu, C.Y. Liu, L. Yin, Q. Kang, L.B. Li, B. Li, *Electrochim. Acta*,
18
19 2014, **133**, 492-500.
20
21
22 28 X.W. Yu, Y.K. Chen, L.P. Chang, L. Zhou, F.X. Tang, X.P. Wu, *Sens. Actuator*
23
24 *B-Chem.*, 2013, **186**, 648-656.
25
26
27 29 X.L. Niu, W. Yang, G.Y. Wang, J. Ren, H. Guo, J.Z. Gao, *Electrochim. Acta*, 2013,
28
29 **98**, 167-175.
30
31
32 30 Y.X. Zhang, Y.X. Cheng, Y.Y. Zhou, B.Y. Li, W. Gu, X.H. Shi, Y.Z. Xian, *Talanta*,
33
34 2013, **107**, 211-218.
35
36
37 31 L.D. Wu, D.H. Deng, J. Jin, X.B. Lu, J.P. Chen, *Biosens. Bioelectron.*, 2012, **35**,
38
39 193-199.
40
41
42 32 D.G. Mita, A. Attanasio, F. Arduini, N. Diano, V. Grano, U. Bencivenga, S. Rossi,
43
44 A. Amine, D. Moscone, *Biosens. Bioelectron.*, 2007, **23**, 60-65.
45
46
47 33 W. Wang, X. Yang, Y.X. Gu, C.F. Ding, J. Wan, *Ionics*, 2015, **21**, 885-893.
48
49
50 34 A.C. Ferrari, J.C. Meyer, V. Scardaci, C. Casiraghi, M. Lazzeri, F. Mauri, S.
51
52 Piscanec, D. Jiang, K.S. Novoselov, S. Roth, A.K. Geim, *Phys. Rev. Lett.*, 2006,
53
54 **97**, 187401(1-4).
55
56
57 35 C. Casiraghi, A. Hartschuh, H. Qian, S. Piscanec, C. Georgi, A. Fasoli, K.S.

1
2
3
4 Novoselov, D.M. Basko, A.C. Ferrari, *Nano Lett.*, 2009, **9**, 1433-1441.
5

6 36 C. Wu, Q. Cheng, K.B. Wu, G. Wu, Q. Li, *Anal. Chim. Acta*, 2014, **825**, 26-33.
7

8 37 C. Wu, Q. Cheng, K.B. Wu, *Anal. Chem.*, 2015, **87**, 3294-3299.
9

10 38 J.T. Zhang, S. Liu, G.L. Pan, G.R. Li, X.P. Gao, *J. Mater. Chem. A*, 2014, **2**,
11 1524-1529.
12
13

14 39 D.A.C. Brownson, J.P. Metters, D.K. Kampouris, C.E. Banks, *Electroanalysis*,
15 2011, **23**, 894-899.
16
17
18
19
20
21
22
23
24
25
26
27
28
29
30
31
32
33
34
35
36
37
38
39
40
41
42
43
44
45
46
47
48
49
50
51
52
53
54
55
56
57
58
59
60

Captions for figures and table

Fig. 1 SEM images of bulk graphite (A), graphite@48 h (B) and TEM image of graphite@48 h (C).

Fig. 2 Raman spectrum (A) and XRD pattern (B) of graphite and graphite@48 h.

Fig. 3 SEM images of CTAB/GCE (A), GS/GCE (B), Ni(OH)₂/GCE (C) and GS-Ni(OH)₂/GCE (D) at high magnification. Scale bar: 1 μm. Inset in Fig. 3C is the low magnification of SEM image of Ni(OH)₂.

Fig. 4 XRD pattern of Ni(OH)₂.

Fig. 5A DPV curves of 0.5 μM BPA at bare GCE (a), CTAB/GCE (b), Ni(OH)₂/GCE (c), GS/GCE (d) and GS-Ni(OH)₂/GCE (e) in 0.1 M phosphate buffer solution (pH 7.5). Fig. 5B Variation of oxidation peak current of 0.5 μM BPA on different electrodes. Accumulation potential: 0.2 V, accumulation time: 120 s, amount of modifier: 2 μL.

Fig. 6 Effect of pH values (A), accumulation potential (B), amount of GS-Ni(OH)₂ suspension (C), and accumulation time (D) on the oxidation peaks current of BPA.

Error bar represents the standard deviation of triple measurements.

1
2
3
4
5
6 Fig. 7A DPV curves of BPA on GS-Ni(OH)₂/GCE with different concentration. Fig.
7
8
9 7B Calibration curve of BPA. Accumulation potential: 0.2 V, accumulation time: 180
10
11 s, amount of modifier: 2 μL. Error bar represents the standard deviation of triple
12
13 measurements.
14
15
16
17
18

19 Table 1 Performance comparison of electrochemical methods for BPA detection.
20
21
22
23

24 Table 2. Determination of BPA in real water samples by GS-Ni(OH)₂ composite.
25
26
27
28
29
30
31
32
33
34
35
36
37
38
39
40
41
42
43
44
45
46
47
48
49
50
51
52
53
54
55
56
57
58
59
60

Fig. 1

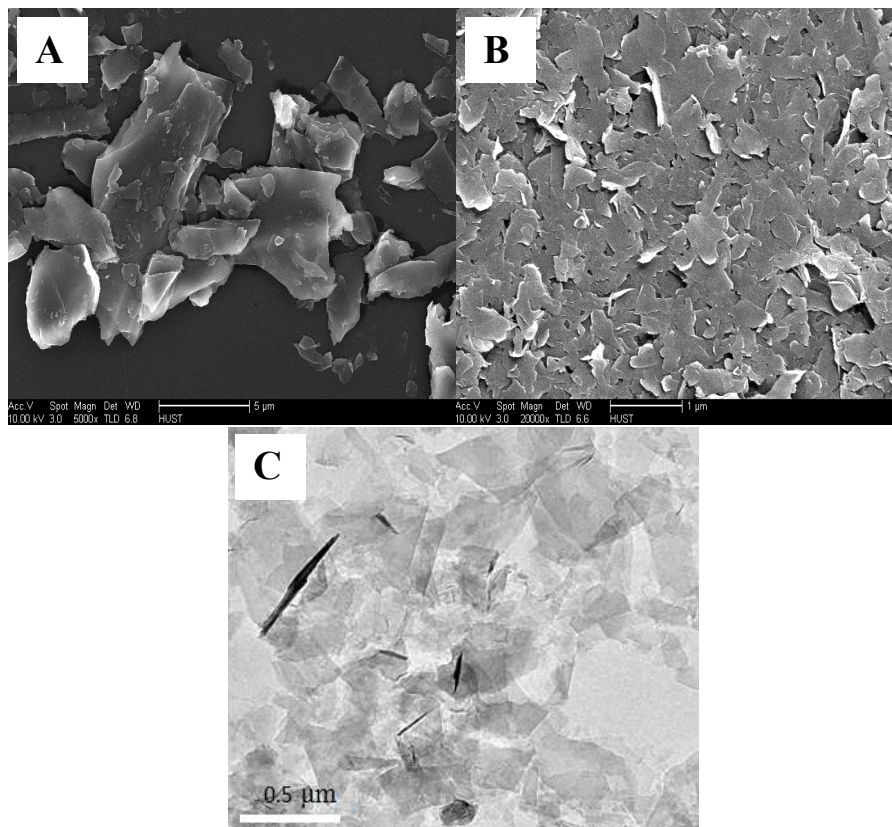


Fig. 2

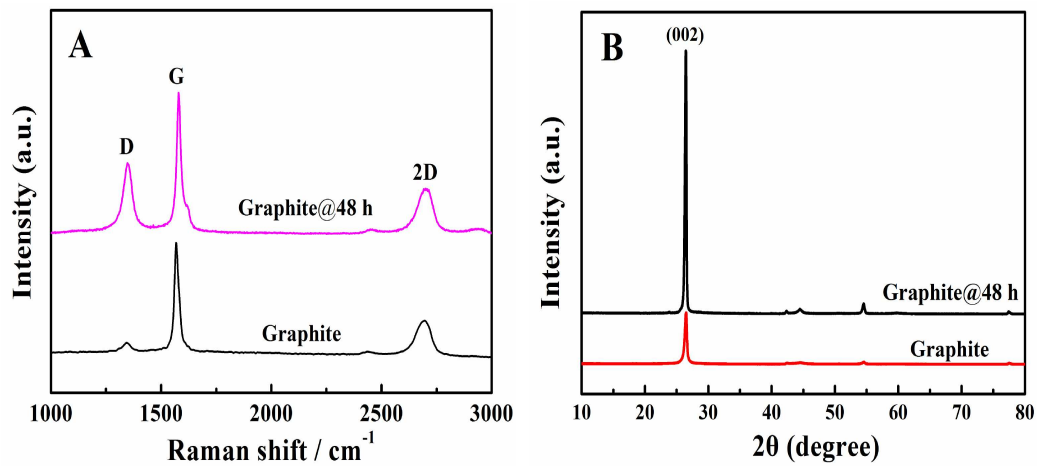


Fig. 3

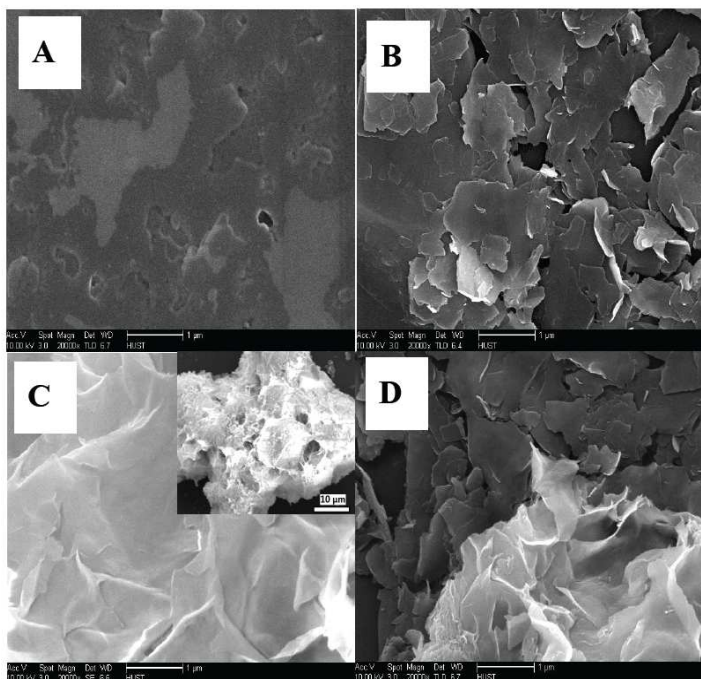


Fig. 4

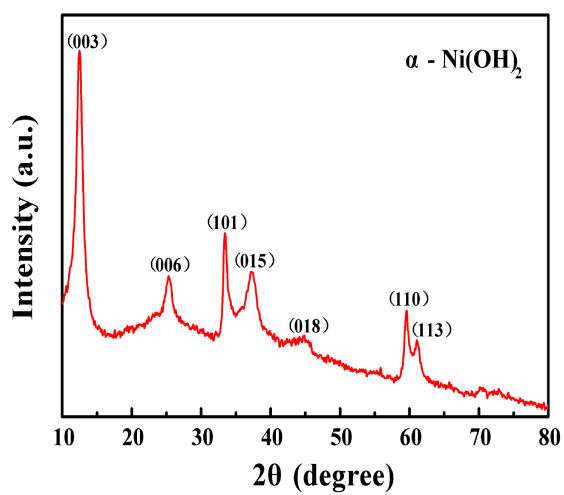


Fig. 5

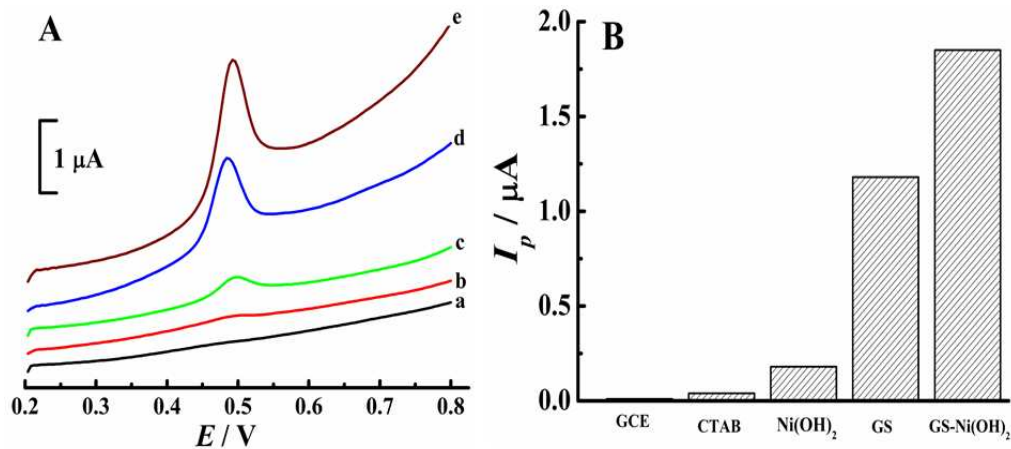


Fig. 6

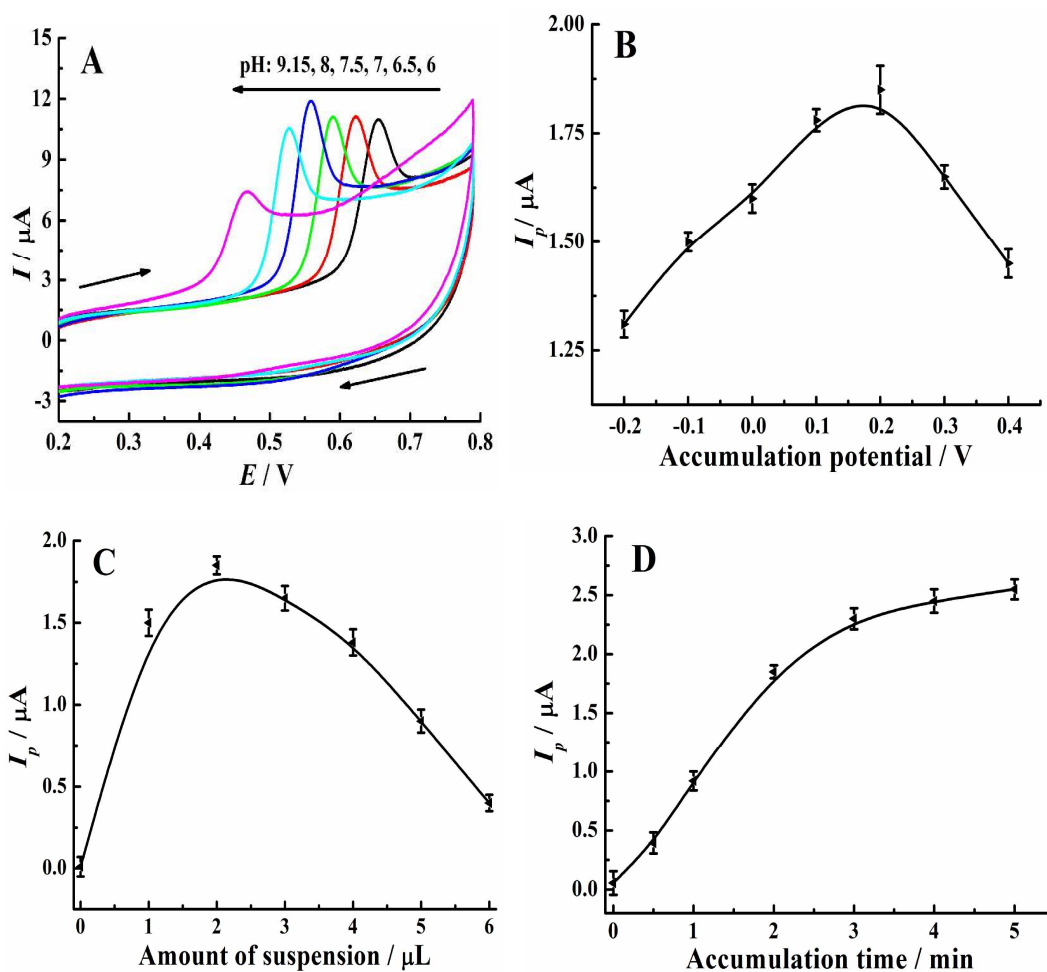


Fig. 7

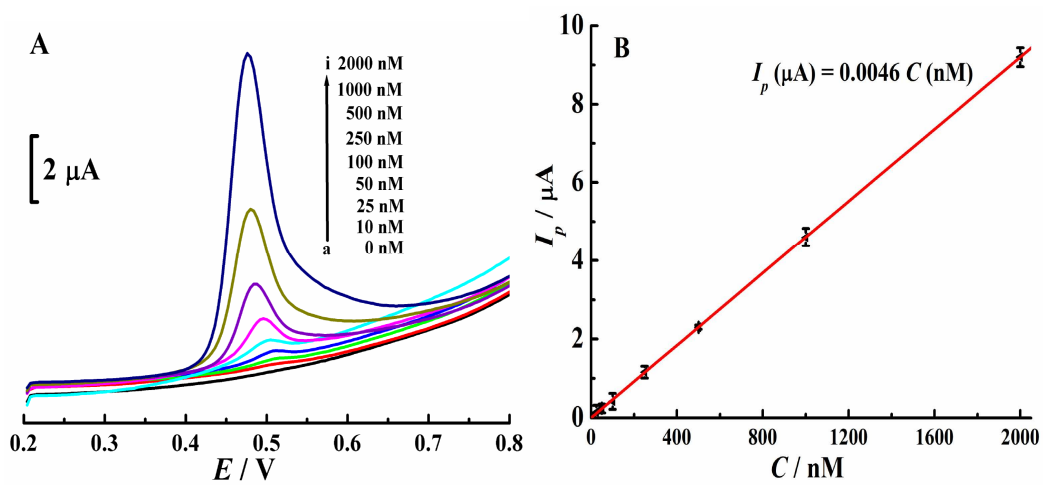
1
2
3
4
5
6
7
8
9
10
11
12
13
14
15
16
17
18
19
20
21
22
23
24
25
26
27
28
29
30
31
32
33
34
35
36
37
38
39
40
41
42
43
44
45
46
47
48
49
50
51
52
53
54
55
56
57
58
59
60

Table 1

Electrodes	Linear range (M)	Detection limit (nM)	References
RGO ^a /GCE	5.0×10^{-8} - 1.0×10^{-6}	47	[24]
Bi ₂ WO ₆ /CPE ^b	7.0×10^{-8} - 1.3×10^{-6}	20	[25]
Mesoporous SiO ₂ /CPE	2.2×10^{-7} - 8.8×10^{-6}	38	[26]
PGA ^c -MWCNT ^d /GCE	1.0×10^{-7} - 1.0×10^{-5}	20	[27]
BMIMBF ₄ ^e /CPE	1.0×10^{-7} - 1.1×10^{-5}	83	[28]
SGNF ^f -Au/GCE	8.0×10^{-8} - 2.5×10^{-4}	35	[29]
MNPs ^g -RGO/GCE	6.0×10^{-8} - 1.1×10^{-5}	17	[30]
Tyrosinase-graphene/GCE	1.0×10^{-7} - 2.0×10^{-6}	33	[31]
Tyrosinase-SWNT ^h /CPE	1.0×10^{-7} - 1.2×10^{-5}	20	[32]
Li ₄ Ti ₅ O ₁₂ -MWCNT/GCE	1.0×10^{-7} - 1.0×10^{-5}	78	[33]
GS-Ni(OH) ₂ /GCE	1.0×10^{-8} - 2.0×10^{-6}	5.0	This work

^a RGO Reduced graphene oxide

^b CPE Carbon paste electrode

^c PGA Polyglutamate acid

^d MWCNT Multi-walled carbon nanotube

^e BMIMBF₄ 1-butyl-3-methylimidazolium tetrafluoroborate

^f SGNF Stacked graphene nanofibers

^g MNPs Magnetic nanoparticles

^h SWCNT Single-walled carbon nanotube

Table 2

Samples	Measured (M)	Spiked (M)	Expected (M)	Founded (M)	RSD (%)	Recovery (%)
1	-	2.0×10^{-8}	2.0×10^{-8}	2.1×10^{-8}	4.2	105.0
2	-	5.0×10^{-8}	5.0×10^{-8}	4.9×10^{-8}	3.8	98.0
3	-	2.0×10^{-7}	2.0×10^{-7}	2.1×10^{-7}	3.4	105.0
4	-	5.0×10^{-7}	5.0×10^{-7}	5.1×10^{-7}	2.7	102.0
5	-	1.0×10^{-6}	1.0×10^{-6}	9.7×10^{-7}	4.5	97.0

Graphical abstract

